Track Reconstruction and Analysis of Alpha Particles in FNTD Dosimeters using Confocal Microscopy

1 Introduction

Fluorescent nuclear track detectors (FNTDs) based on Al_2O_3:C,Mg single crystals can reconstruct individual charged particle trajectories through confocal fluorescence microscopy (CFM) readout [1, 2]. In an FNTD, a traversing ion deposits energy along its path, ionising the crystal and leaving metastable colour centres (aggregates of oxygen vacancies, of which the F_2^{2+} centre is the most relevant). During readout, a focused laser beam is scanned point-by-point across the sample in a confocal microscope; fluorescence emitted only from the in-focus plane passes through a pinhole and reaches the detector, rejecting out-of-focus light. By stepping the focus along the optical axis a three-dimensional stack of optical sections is recorded, and the same colour centres are sampled again. The correlation of the resulting fluorescent spots across focal planes yields the 3D track geometry, from which particle fluence, incidence angle, and energy can be derived [3].

This report analyses confocal z-stacks of FNTDs irradiated with alpha particles from a U-232 source (a multien-ergetic 5–7 MeV source; Section 2.1), acquired on several dates between November and December 2025. The methodology follows Kouwenberg et al. [3] in automated spot detection and linking, with SRIM-2013 [5] range-to-energy conversion. It is important to stress that the results reported here are preliminary: several inconsistencies between the measured track depths and the SRIM expectations (Sections 2.5 and 4) suggest that the acquisition may not have captured full particle tracks, and the measurements may need to be repeated. We therefore treat the quantitative results with caution. The analysis and figure-generation code used throughout this report is openly available at https://github.com/astroanax/fntd-track-reconstruction.

2 Methods

2.1 Irradiation and acquisition geometry

The samples were irradiated with alpha sources and read out on a Leica SP5 confocal microscope using 633 nm and 488 nm excitation. Table 1 summarises the irradiation history as recorded in the laboratory notes. Three of the four datasets analysed here (20251112, 20251114, 20251210) used a U-232 source, which emits a multien-ergetic spectrum of alpha particles in the 5–7 MeV range, *not* the monochromatic ∼5 MeV Am-241 emission. Only datasets 20260225 and 20260309 (not analysed here) used an Am-241 source. All irradiations were performed in vacuum ($\sim 1 \times 10^{-2}$ mbar) so that, in the absence of a degradation foil, essentially no energy loss is expected between source and detector.

Table 1: Irradiation history. d = source-to-crystal distance; "Mylar" = 6 μm Mylar degradation foil. Al_2O_3:C,Mg is the FNTD material unless stated otherwise.

Dataset	Source	Activity	Time	d	Foil
20251112 (12/11)	U-232	13 kBq	5 h	13.4 cm	none
20251114 (14/11)	U-232	13 kBq	24 h	—	—
20251119 (19/11)	*LiF detector, WF readout*	—	—	—	—
20251210 (10/12)	U-232	13 kBq	24 h	4–4.5 cm	6 μm
20260211 (11/02)	U-232	13 kBq	41 h	1.5 cm	6 μm
20260225 (25/02)	Am-241	1 kBq	24 h	1 cm	6 μm
20260309 (09/03)	Am-241	1 kBq	68–70 h	1 cm	6 μm

2.2 Datasets

Tables 2–5 give the series inventory. The columns are: Series number (S), series name, excitation wavelength (λ), image size in pixels, number of Z-planes (Z), number of colour channels (C, where present), and bit depth. Z is the number of focal planes (axial positions) in the stack; it is not a time dimension. Series are included only where stated as analysed. Each dataset is accompanied by a .lifext file containing photon-counting data from a Photon Multiplier Detector (PMD); see Section 3.6.

Two important caveats apply to the comparison. First, the 20251119 dataset is not an Al_2O_3:C,Mg FNTD: it corresponds to a **wide-field (WF)** readout of a **LiF (lithium fluoride) detector** that was not irradiated by us. It is therefore *not* comparable with the confocal Al_2O_3 measurements and is treated separately (Section 3.3). Second, any series acquired in wide-field mode (e.g. 20251112 S6) is not a confocal stack and must not be compared directly with the confocal series; it is discussed in its own sub-section.

Table 2: 20251112.lif (acquired 2025-11-12, 7.4 GB), U-232. All series 8-bit except S6 (16-bit). WF = wide-field.

S	Name	λ (nm)	Size (px)	Z	bits
1	633_40x	633	1024^2	14	8
2	633_63x	633	1024^2	52	8
3	633_63x_01	633	512^2	52	8
4	633_63x_02	633	512^2	130	8
5	488_63x_00	488	1024^2	76	8
6	488_63x_WF	488	1392×1040	2583	16
7	Series009	—	1024^2	1	8
8	Series010	—	1024^2	5	8
9	488_63x_Conf	488	512^2	1000	8

Table 3: 20251114.lif (acquired 2025-11-14), U-232. S6 was recorded without irradiation, but we note that no dedicated control measurement is present in the laboratory records, so this series should not be treated as a definitive unirradiated control.

S	Name	Size (px)	Z	C	bits
1	Series003	1352^2	241	1	8
2	00_xy	1800^2	1	2	8
3	00_xz	1800^2	1	2	8
4	y-stack	744^2	216	2	8
5	wf_z-stack	2048^2	260	2	16
6	wf_no_irrad.	2048^2	260	2	16

Table 4: 20251119.lif (acquired 2025-11-19). *This is a LiF detector read out in wide-field mode*, not an Al_2O_3:C,Mg confocal measurement; it was not irradiated by us. Treated separately in Section 3.3.

S	Name	Size (px)	Z	C	bits
1	alumina_01_20x	512^2	334	2	8
2	alumina_01_63x	512^2	334	2	8
3	Series003	1392×1040	43	1	16
4	Series004	1392×1040	41	1	16
5	Series005	2048×1024	72	1	8
6	Series006	2048×1024	95	1	16
7	Series007	2048^2	76	1	16
8	Series008	2048^2	12	1	16
9	Series009	512^2	74	1	16

Table 5: 20251210.lif (acquired 2025-12-10), U-232, 6 μm Mylar. Tile scans with 25 positions (S1–S25, S27–S51) and the stitched/mosaicked composite images (S26, S52, labelled "merged"). All 1336^2 tiles × 2 channels, 8-bit.

Series	Type	Size (px)	Z	C
S1–S25	Tiles 1–25	1336^2	21	2
S26	Merged (stitched)	4173^2	21	2
S27–S51	Tiles 1–25	1336^2	28	2
S52	Merged (stitched)	4172×4173	28	2

2.3 SRIM Simulation

The projected range and electronic stopping power of He-4 ions in Al_2O_3 (density 3.98 g/cm^3) were computed with SRIM-2013 [5] using 999 ions at 5 MeV, the lower bound of the U-232 spectrum. The mean projected range is 13.5 μm with 0.21 μm straggling. Entry LET is 267 keV/μm, rising to a Bragg peak of 590 keV/μm at 11.7 μm. Because the source is multienergetic, this single 5 MeV curve should be taken as a reference only: a 7 MeV alpha would have a correspondingly longer range (∼19–20 μm) and its Bragg peak would lie deeper.

Regarding the energy-loss mechanism: nuclear (elastic) stopping accounts for only 0.06% of the total energy loss at these energies. The remaining 99.94% is *electronic* stopping, in which the alpha transfers energy to target electrons by excitation and ionisation. The ionised electrons are precisely what creates the colour centres (the F_2^{2+} signal) that constitute the visible track; the small residual nuclear contribution consists of occasional large-angle elastic collisions with target nuclei, which are responsible for the (small) lateral straggling and for the fact that an alpha's path is not perfectly straight.

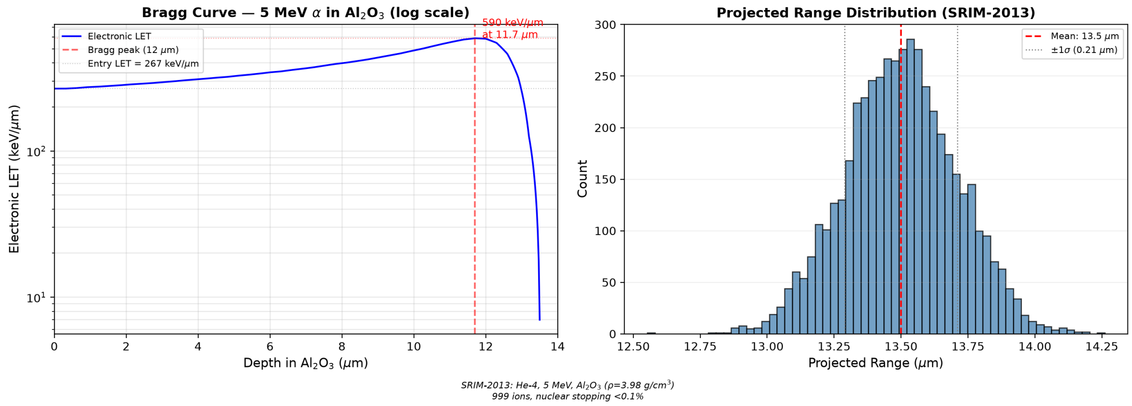

Figure 1: Left: Bragg curve (log scale) from SRIM-2013 IONIZ.txt at 5 MeV. Right: Projected range histogram (mean 13.5 μm, 0.21 μm straggling).

2.4 Track Reconstruction

Image analysis was performed in Fiji/ImageJ [7] using a custom Jython script and the TrackMate v7.14 plugin [6]. Each confocal series was loaded via Bio-Formats [8]. TrackMate operates on a time series, so the third spatial dimension (the Z-planes of the stack) is mapped onto the time axis via a Z→T swap (HyperStackConverter). Here Z denotes the focal-plane index within the stack (an axial position), while T is the TrackMate frame index after the swap; "tracking across frames" therefore corresponds to linking spots between consecutive focal planes. Multi-channel series were reduced to a single channel: only channel 1 (the 633 nm channel for the Al_2O_3 FNTD) was used, and the remaining channels were discarded. Spots were detected with an intensity threshold detector. The threshold was set to 2 for 8-bit images, 600 for 16-bit images, and 30 for the brighter 8-bit 20251114 and 20251210 datasets, selected based on per-dataset image statistics. Spot linking used the Simple Sparse LAP tracker with a maximum linking distance of 20–30 pixels and zero frame gaps. The analysis pipeline is implemented in a mixture of languages: the image-processing step runs inside Fiji as a Jython script, while the geometry, SRIM interpolation, filtering, and plotting are done in Python (numpy/scipy/pandas/matplotlib); the two are coupled through CSV files; the full pipeline, with the exact commands needed to reproduce every figure and result, is documented in the accompanying `README.md`.

Alpha particles are heavy ($M_\alpha \approx 4$ u) and, over the depth range probed here, lose energy predominantly by electronic stopping, so their trajectory through the crystal is essentially a straight line unless they happen to pass close enough to a nucleus to undergo a large-angle elastic scatter. Track straightness is therefore a physically meaningful quality metric for these tracks (Section 2.5).

Post-processing computes for each track: 3D length (sum of stepwise Euclidean distances between consecutive spots along the track), incidence angle from the surface normal ($\theta = \arccos(|\Delta z|/L_{\mathrm{disp}})$ where L_{disp} is the straight-line displacement from first to last spot), and per-spot pixel intensity from the raw image in a 7×7 neighbourhood. Track straightness is defined as the ratio of displacement to total path length, $S = L_{\mathrm{disp}}/L_{\mathrm{path}}$, where $L_{\mathrm{path}} = \sum_i \sqrt{(x_{i+1} - x_i)^2 + (y_{i+1} - y_i)^2 + (z_{i+1} - z_i)^2}$. $S = 1$ indicates a perfectly straight track; $S < 1$ indicates deviation from linearity. A track must contain at least three spots to define a well-constrained 3D direction, and series yielding fewer than two reconstructed tracks are excluded from the statistical summaries because a sample of one (or zero) is insufficient. SRIM-derived remaining energy and LET are evaluated at the track endpoints via interpolation of IONIZ.txt.

2.5 Track depth and the "half-in, half-out" scan

Because the scan is started with the focal plane above the crystal surface, only roughly the upper half of the stack lies inside the crystal; the rest is in air (and possibly a cover slip). This has a decisive consequence for the interpretation of track length. If an alpha enters at a steep angle, the portion of its track captured by the confocal stack is only the segment that falls inside the scanned depth—typically the part nearer the surface, before the Bragg peak is reached, where the LET is still low and the signal may be weak. The measured track depth is therefore expected to be *shorter* than the full SRIM range, and the apparent track length and the depth at which spots appear must be examined against this truncation. We report the axial extent of each track (Z-extent, μm) in Table 6 to allow this comparison.

3 Results

3.1 Track Length Distributions

Figure 2 shows the track length distribution for each successfully processed confocal series. Table 6 summarises the complete results, including the track Z-extent. Series with fewer than 2 tracks, single-plane images, tile scans, or non-standard axis ordering were excluded from processing.

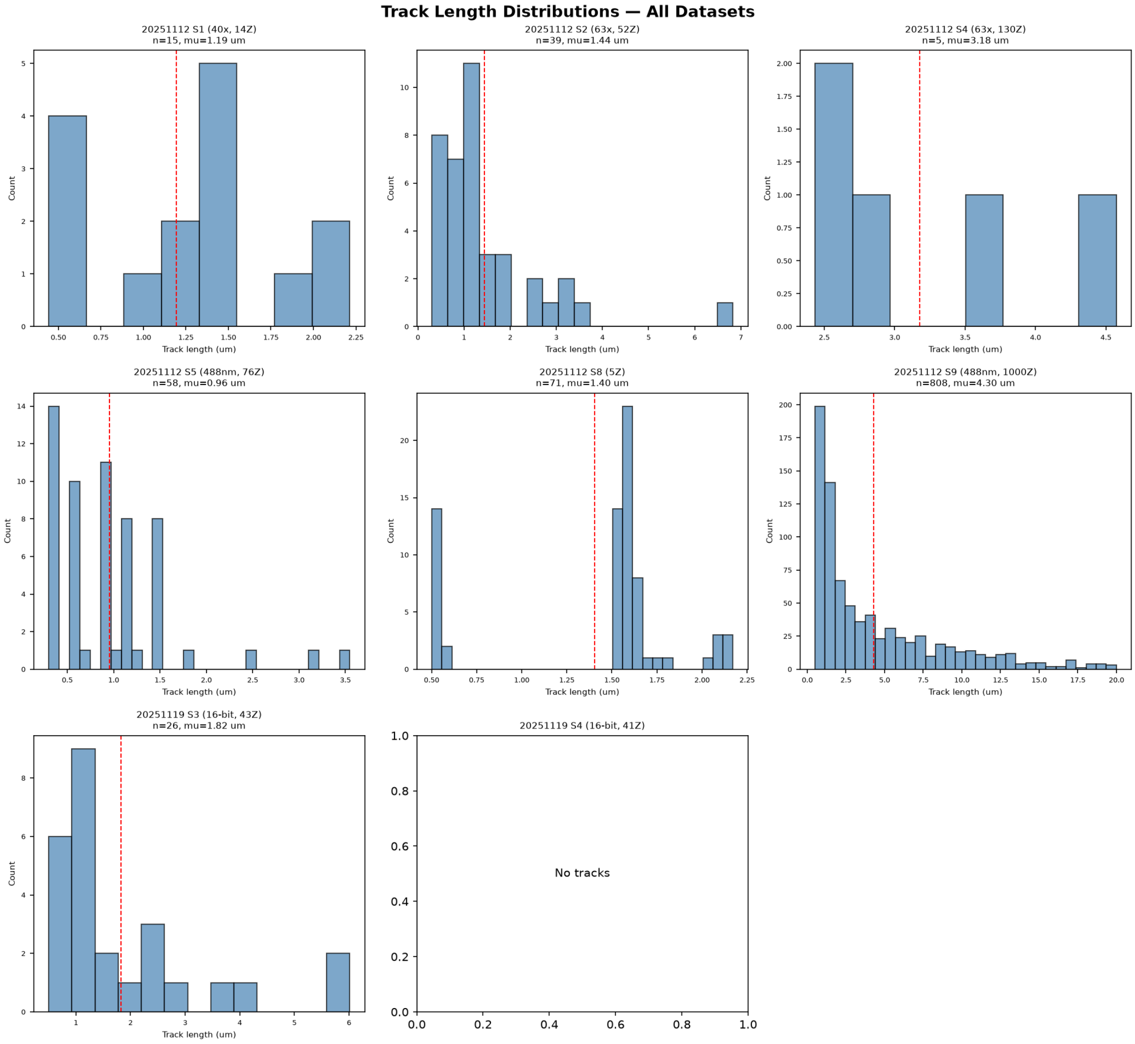

Figure 2: Track length distributions across all processed confocal series.

Table 6: Complete track reconstruction results. Values are mean ± standard deviation. Z-extent is the axial (depth) span of the tracks. "—" = not processable or not applicable. Datasets acquired 2025-11-12, 2025-11-14, 2025-11-19, 2025-12-10. *Only 633 nm confocal Al_2O_3 series are directly comparable*; 488 nm and WF series are discussed separately.

Dataset & Series	Tracks	Length (μm)	Z-extent (μm)	Angle (°)	Spots/trk
20251112 S1 (40×, 14Z)	15	1.19 ± 0.58	0.91	23 ± 31	3.1 ± 1.3
20251112 S2 (63×, 52Z)	39	1.44 ± 1.22	0.64	50 ± 21	3.2 ± 1.7
20251112 S3 (63×, 52Z)	5612	4.92 ± 1.99	0.58	81 ± 8	3.0 ± 0.6
20251112 S4 (63×, 130Z)	5	3.18 ± 0.92	3.10	2.8 ± 1.7	11.4 ± 2.7
20251112 S5 (488 nm, 76Z)	58	0.96 ± 0.66	0.85	9.4 ± 17.3	3.9 ± 1.8
20251112 S6 (WF, 2583Z)	1	—	—	—	2583
20251112 S8 (5Z)	71	1.40 ± 0.50	1.32	9.7 ± 6.6	3.6 ± 0.9
20251112 S9 (488 nm, 1000Z)	840	5.13 ± 6.16	3.64	27 ± 21	8.3 ± 9.5
20251114 S6 (unirrad.)	0	—	—	—	—
20251119 S3 (LiF, WF)	26	1.82 ± 1.57	1.54	14 ± 25	4.1 ± 3.0
20251119 S4 (LiF, WF)	1	20.0	20.0	0.0	41
20251210 S2 (merged)	—	—	—	—	—

3.2 633 nm confocal Al_2O_3 series

3.2.1 Variation among the 633 nm series

For the Al_2O_3 FNTD, only the 633 nm readout is of interest, since it selectively excites the particle-induced F_2^{2+} centres. Among the 633 nm confocal series, the measured mean track length is short (1–3 μm) compared with the SRIM range of 13.5 μm, and the Z-extent (0.6–3.1 μm) is likewise far below the full range. Two series deserve comment.

Series 3 of 20251112 (5612 raw tracks, 0.34 μm/px) is effectively eliminated by the Kouwenberg filters (Table 8): only 0.04% pass. The dominant filter is angle ($\leq 50°$), which removes 5605 of 5612 tracks. The raw population has a mean angle of $81° \pm 8°$, incompatible with alpha tracks that should be preferentially aligned near the surface normal. At 6× coarser pixels than series 2, the threshold detector flags dark-current noise as spots; the LAP linker chains them randomly across 52 planes. The 2 surviving tracks (length 0.91 μm, angle 5.6°) may be genuine but are too short for reliable dosimetry. This series is excluded from further analysis.

Series 4 (20251112, 633 nm, 130 Z) yields only 5 tracks, but they are near-perpendicular (2.8° from normal), long (3.2 μm) and span many planes (11.4 spots), giving the largest Z-extent (3.1 μm). The deep scan captures more of each track. Yet even these 5 tracks fall well short of the 13.5 μm SRIM range, which is the central discrepancy discussed in Section 4.

3.2.2 The 488 nm series

Because only 633 nm selectively excites the F_2^{2+} colour centres of an Al_2O_3 FNTD, the 488 nm series (S5, S9) are expected to show no particle response and are set apart here rather than compared directly. Series 5 (488 nm, 76Z) retains 48% after filtering; the tracks have extremely shallow angles ($4.4° \pm 10.3°$) despite the wrong excitation, which suggests either co-localisation with real alpha-induced defects that weakly fluoresce at 488 nm, or stitching artefacts of the confocal stage. Series 9 (488 nm confocal, 1000Z) retains 56%, but its filtered length (8.2 ± 6.8 μm, Z-extent up to 42 μm) is problematic: the long chains through 1000 confocal planes likely stitch together independent fluorescent spots from different crystal locations into spurious long tracks. These 488 nm results should be regarded as an experiment confirming that the wrong wavelength gives an awkward, non-physical response, not as a quantitative alpha measurement.

3.2.3 The wide-field series

Series 6 of 20251112 (488 nm, wide-field, 16-bit, 2583 planes) produced a single 2583-spot "track" with perfect straightness. This is a detection artefact: in wide-field mode the image lacks the optical sectioning of a confocal acquisition, so the same bright background is present in every plane and is linked into one chain. A wide-field readout is not confocal and cannot be analysed with the confocal tracking approach or compared with the confocal series; it is reported here only to confirm that the wide-field configuration is unsuitable for this particle-tracking analysis.

3.3 LiF detector (20251119)

The 2025-11-19 dataset is a special case: it is a **LiF detector** read out in **wide-field mode**, and it was *not* irradiated by us. It is therefore not an Al_2O_3:C,Mg confocal measurement and is not comparable with the other datasets. We report the raw tracking outcome for completeness. Series 3 (43 planes, 1392×1040, 0.146 μm/px, 0.500 μm Z-step) yielded 26 tracks with much higher intensity than the 8-bit Al_2O_3 data (Table 7); Series 4 contains a single track penetrating all 41 planes (20 μm). Because the detector material (LiF, $\rho \approx 2.64$ g/cm^3) and readout mode differ from Al_2O_3 confocal, the SRIM range used for Al_2O_3 (13.5 μm) does *not* apply here, and these tracks should not be compared with the confocal results. They are shown only because the data exist.

Table 7: Intensity comparison between the 8-bit Al_2O_3 confocal series 2 (20251112) and the wide-field LiF series 3 (20251119). These are different detectors and readout modes and are *not* directly comparable; the table only illustrates the intensity difference.

Metric	20251112 S2 (8-bit confocal)	20251119 S3 (LiF WF)
Tracks	39	26
Length (μm)	1.44 ± 1.22	1.82 ± 1.57
Angle (°)	50 ± 21	14 ± 25
Spots/track	3.2 ± 1.7	4.1 ± 3.0
Mean pixel intensity	0.48 ± 0.29	407 ± 9
Sum local intensity	63 ± 39	76,351 ± 51,029

3.4 Kouwenberg Filtering

To assess the quality of reconstructed tracks, we applied the three post-filtering criteria from Kouwenberg et al. [3]: (1) spot count ≥ 4 per track (relaxed from ≥ 8 for our shorter tracks due to partial scan depth), (2) fitted incidence angle $\leq 50°$ from surface normal, and (3) intensity similarity: all spots within a track must have pixel intensities within 3σ of the track mean (Table 8). The filters remove tracks that are too short, too oblique, or have inconsistent intensities, and are used to identify which series contain genuine, well-formed alpha tracks.

Table 8: Kouwenberg 2016 filter results. S3 is eliminated; the 488 nm series are partially retained but are not valid alpha measurements (Section 3.2.2).

Series	Raw tracks	After filters	Retained (%)	Filtered length (μm)
20251112 S2 (633 nm, 63×)	39	8	21%	2.84 ± 1.85
20251112 S3 (633 nm, coarse px)	5612	2	0.04%	0.91 ± 0.01
20251112 S4 (633 nm, 130Z)	5	5	100%	3.18 ± 0.92
20251112 S5 (488 nm, 76Z)	58	28	48%	1.40 ± 0.66
20251112 S9 (488 nm, 1000Z)	840	470	56%	8.20 ± 6.79
20251119 S3 (LiF, WF)	26	8	31%	3.26 ± 1.84

3.5 MOSAIC Particle Tracker Comparison

To evaluate whether the MOSAIC Particle Tracker [3] improves track detection, the 20251112 Series 2 data was also processed in Fiji using the MOSAIC Particle Tracker 2D/3D plugin (settings: kernel radius = 5, cutoff = 0.0, percentile = 0.01, displacement = 20 px, link range = 2). The link range of 2 was selected over 3 because link range 3 produced 633 tracks with visibly squiggly trajectories, indicative of false cross-linking. Alpha tracks are expected to be straight (straightness $S \approx 0.8$–1.0); a higher link range permits connections across up to 3 missing frames, which for continuous alpha tracks creates more false links than genuine reconnections.

Table 9: MOSAIC Particle Tracker vs. TrackMate comparison for 20251112 Series 2 (633 nm, 63×, 52Z, link range = 2). Identical Kouwenberg filters applied ($\geq$ 4 spots, $\leq 50°$, $\leq 3\sigma$ intensity).

Method	Raw tracks	After filters	Retained	Length (μm)	Angle (°)
MOSAIC (link range 2)	509	4	0.8%	3.70 ± 0.97	38.9 ± 9.0
TrackMate (threshold)	39	8	20.5%	2.84 ± 1.85	25.0 ± 13.5

MOSAIC detects 509 tracks versus TrackMate's 39, but 84% of MOSAIC trajectories are only 2-spot pairs, which the angle filter eliminates. TrackMate's intensity threshold detector is more selective, producing longer, more physically plausible tracks. After filtering, both methods converge to a similar number of high-quality tracks (4 vs. 8). TrackMate is preferred as it produces tracks with fewer spurious 2-spot fragments and operates in automated headless mode.

Figures 3 and 4 show three-dimensional track reconstructions for the key series. Each coloured line represents a linked chain of detected spots across consecutive Z-planes.

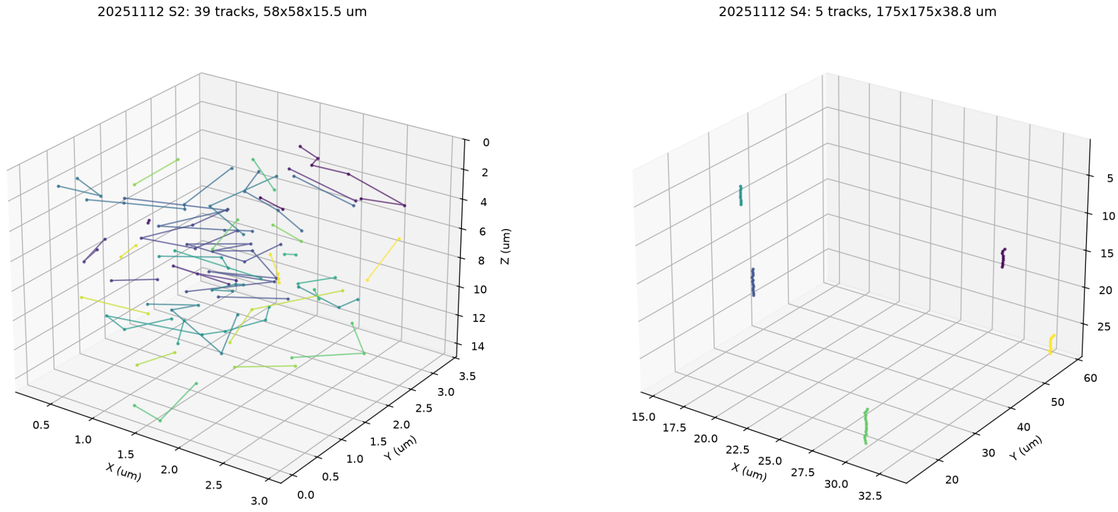

(a) 20251112 S2: 39 tracks

(b) 20251112 S4: 5 tracks

Figure 3: 2025-11-12 dataset, 633 nm confocal channel.

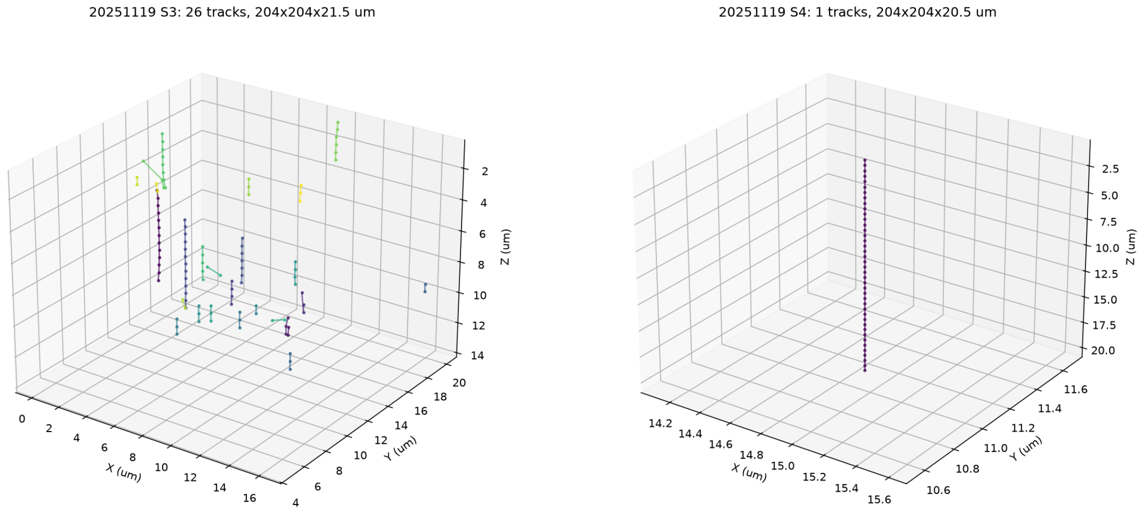

(a) 20251119 S3 (LiF, WF): 26 tracks

(b) 20251119 S4 (LiF, WF): 1 track, 20 μm

Figure 4: 2025-11-19 dataset (LiF, wide-field readout).

3.6 Extended Metadata (lifext)

All datasets contain companion .lifext files providing photon-counting data from a Photon Multiplier Detector (PMD) (Table 10). Each file contains a histogram of photon counts and 2–3 PMD channels at progressively lower resolutions. The PMD records per-voxel photon arrival rates, independent of the 8-bit/16-bit imaging channel.

Table 10: PMD photon-counting data. Max counts shown for the highest-resolution PMD channel (pmd_0).

Dataset	PMD channels	pmd_0 size (px)	Max photon counts
2025-11-12	2	512^2	3
2025-11-14	3	676^2	96
2025-11-19	3	256^2	255 (saturated)
2025-12-10	2	668^2	131

The 2025-11-12 dataset shows only 1–3 photon counts per voxel, consistent with its extremely low 8-bit signal. The 2025-11-19 dataset reaches saturated photon counting (max 255), reflecting its much higher fluorescence yield.

3.7 Fluence and Energy

Table 11 gives track fluence and estimated initial alpha energy for the 633 nm confocal Al_2O_3 series. Fluence is computed as tracks divided by the imaged area, corrected for the maximum accepted incidence angle per [3]; the remaining energy is obtained by interpolating the 5 MeV SRIM curve at the track endpoints. The fluence varies by almost two orders of magnitude across the series (135 to 11,480 mm^{-2}). This large spread reflects differences in source-to-detector distance (the solid angle subtended by the detector), exposure time, and readout magnification, and the fact that only a fraction of each track is detected; it is not a single reproducible fluence value. These numbers should therefore be treated as order-of-magnitude estimates.

Table 11: Dosimetric quantities for the 633 nm confocal channel. Fluence varies by orders of magnitude because of different source geometry, exposure, and scan depth; see text.

Series	Tracks	Fluence (mm^{-2})	E_{est} (MeV)
20251112 S1 (40×)	15	3170	5.0 ± 0.1
20251112 S2 (63×)	39	11480	4.8 ± 0.7
20251112 S4 (63×)	5	163	5.1 ± 0.2

4 Discussion

The pipeline successfully reconstructs alpha particle tracks from confocal FNTD images, extracting fluence, incidence angle, and approximate energy. However, the central finding is a discrepancy that we cannot fully resolve with the present data: the measured track depths (Z-extent 0.6–3.1 μm) and lengths (1–3 μm) are far shorter than the SRIM range of 13.5 μm for a 5 MeV alpha in Al_2O_3. There are two plausible explanations, which are not mutually exclusive.

First, the "half-in, half-out" scan geometry truncates the tracks. If the scan begins above the crystal surface, the captured segment is only the part of the track that lies inside the scanned depth. In the meeting of 2025-09-01 this was examined explicitly: the professor noted that before half of the stack we are in air, that we may not have enough sensitivity to see the region where the LET is low, and that the tracks appear too short (they should be ~8–10 μm, not 1–3 μm). The lack of sensitivity of the detection/acquisition system at low LET—i.e., near the beginning of the track, before the Bragg peak—is a likely reason we do not see the full alpha path. Under this hypothesis the data are not wrong per se, but the visible segment is only the (higher-LET) tail of each track, and the full track is not recorded.

Second, and more cautiously, the data themselves may be unreliable or the experimental records incomplete. The professor explicitly raised the possibility that "the data is wrong" and urged that we be critical of the result and that the measurements be repeated. We therefore do not claim a definitive measurement of alpha range or energy; the energy estimates in Table 11 (which happen to return ∼5 MeV) are a consequence of interpolating the 5 MeV curve at the shallow observed depths and do *not* by themselves validate the source energy, since the track begins already part-way along its path. In particular, the near-∼5 MeV values should not be over-interpreted.

Several other points limit the comparison and the analysis:

- The 20251119 dataset is a LiF detector read out in wide-field mode and was not irradiated by us. It is a different detector and readout configuration and is *not* comparable with the Al_2O_3 confocal measurements.
- Wide-field series (20251112 S6) and the 488 nm series (S5, S9) are not valid 633 nm-confocal alpha measurements and are discussed only as experiments confirming their unsuitability.
- The experiment is performed in vacuum ($\sim 10^{-2}$ mbar), so little energy loss is expected in the path; if unexpected energy loss occurred (e.g. due to a degradation foil or air), it would shift the effective source energy, which is not accounted for in the 5 MeV reference curve.
- The TrackMate distance-only LAP tracker is a simplified approximation of the four-feature MOSAIC-based algorithm developed specifically for ion tracks [3]; using the published Fiji plugin would improve linking accuracy, particularly for intensity-based energy estimation.
- The PMD photon-counting data in the lifext files is entirely unutilised and could provide the quantitative per-track intensity calibration needed for LET spectrometry.
- No dedicated unirradiated control is present in the records, so we cannot independently confirm zero false positives from the pipeline.

In light of these caveats, we consider the current results preliminary. The measurements should be repeated with a scan that starts inside the crystal, spans the full depth, and is aligned so that complete tracks (or at least the region through the Bragg peak) are captured. Only then can track length be compared quantitatively with the SRIM range and an energy/LET determination be made reliably.

5 Conclusion

Alpha particle tracks were reconstructed from confocal FNTD images using Fiji/TrackMate and SRIM-2013 range-to-energy conversion. In the 633 nm readout channel of Al_2O_3:C,Mg, the detected tracks have mean lengths of roughly 1–3 μm and axial extents below 3.1 μm, well short of the 13.5 μm SRIM range of a 5 MeV alpha. Because the measured track depth is inconsistent with the expected full range, and because the acquisition starts above the crystal surface and may lack sensitivity at low LET, we cannot conclude that a full, reliable alpha track measurement was achieved; the data are preliminary and the measurements should be repeated with a scan geometry that captures complete tracks. The 20251119 dataset is a LiF detector with a wide-field readout and is not comparable to the Al_2O_3 confocal measurements. The pipeline itself performs the intended detection, filtering, and SRIM-based analysis, and the 16-bit wide-field/LiF data demonstrate the substantially higher fluorescence signal available in that configuration. Integration of PMD photon-counting data and implementation of the MOSAIC-based Kouwenberg tracker [3] are identified as next steps.

References

[1] M.S. Akselrod, G.J. Sykes Kramer, and T.H. Williams. Fluorescent nuclear track detector technology. *Rev. Sci. Instrum.*, 82(2):023501, 2011.

[2] G.M. Akselrod, M.S. Akselrod, E.R. Benton, and N. Yasuda. A novel Al_2O_3 fluorescent nuclear track detector for heavy charged particles and neutrons. *Nucl. Instrum. Meth. B*, 247(2):295–306, 2006.

[3] J.J.M. Kouwenberg, L. Ulrich, O. Jäkel, and S. Greilich. A 3D feature point tracking method for ion radiation. *Phys. Med. Biol.*, 61(11):4088–4104, 2016.

[4] I.D. Muñoz, S. Greilich, O. Jäkel, and J.J.M. Kouwenberg. Sensitivity correction of fluorescent nuclear track detectors using alpha particles. *Med. Phys.*, 50(4):2386–2400, 2023.

[5] J.F. Ziegler, M.D. Ziegler, and J.P. Biersack. SRIM — The stopping and range of ions in matter (2010). *Nucl. Instrum. Meth. B*, 268(11–12):1818–1823, 2010.

[6] J.-Y. Tinevez, N. Perry, J. Schindelin, et al. TrackMate: An open and extensible platform for single-particle tracking. *Methods*, 115:80–90, 2017.

[7] J. Schindelin, I. Arganda-Carreras, E. Frise, et al. Fiji: an open-source platform for biological-image analysis. *Nature Methods*, 9(7):676–682, 2012.

[8] M. Linkert, C.T. Rueden, C. Allen, et al. Metadata matters: access to image data in the real world. *J. Cell Biol.*, 189(5):777–782, 2010.